Available online at www.sciencedirect.com

ScienceDirect

Procedia Structural Integrity 12 (2018) 538–552

Structural Integrity Procedia

www.elsevier.com/locate/procedia

AIAS 2018 International Conference on Stress Analysis

# A continuous model for the railway track analysis in the lateral plane

M. Catena[a], A. Gesualdo[b], S. Lisi[a], F. Penta[c,*], G.P. Pucillo[c]

[a]*Technical Management / Technological and Experimental Standard - Superstructure, Rete Ferroviaria Italiana - RFI S.p.A., Piazza della Croce Rossa 1, 00161, Rome, Italy*

[b]*Department of Structures for Engineering and Architecture, University of Naples Federico II, via Claudio 21, 80125 Naples, Italy*

[c]*Department of Industrial Engineering, University of Naples Federico II, Piazzale Tecchio 80, 80125 Naples, Italy*

**Abstract**

This paper deals with a mechanical model for the analysis of the railway track behaviour built by exploiting the periodicity of the track-structure. The starting point of this study is the analysis of the inner forces transferring modes. They have been determined by the unit principal vectors analysis of the base cell transfer matrix.

The proposed model is able to reproduce accurately the track behaviour in transferring its inner forces. However, solutions that are equilibrated but not kinematically admissible are obtained from it when transversal loads are applied. In additions, only boundary conditions compatibles with the track transferring modes can be satisfied. This inconsistency is eliminated by superposition of a corrective deformed shape. This is derived from the eigenvectors of the transfer matrix pertaining to self-equilibrated systems of bending moments decaying along the track.

The application field of the proposed track model is also discussed and the results of a validation study carried out by F.E. analysis are finally presented.



*Keywords:* Periodic beam-like structure; Homogenization; Transfer state matrix eigen-analysis; Continuous welded rail; Railway track model

## 1. Introduction

Although over the last three decades most of the railway tracks have been built by the continuous welded rail technique, several technical problems still prevent the full achievement of the best performance of this constructive solution in terms of maintainability, energy consumption reduction, comfort degree offered to the passengers and lifetime of the rails and rolling stock. Surely, a key role is played by the natural trend of this system toward the thermal buckling phenomenon and, even more so, the unpredictability of the thermal and mechanical conditions in which this phenomenon may occur.

*Corresponding author. Tel.: +39-(0)81-7682451; cell: +39-347-6080985.
*E-mail address:* penta@unina.it


10.1016/j.prostr.2018.11.065

Most of the predictive models until now proposed were implemented in advanced computer aided engineering (*cae*) environments, see Esveld and Hengstum (1988); Jackson et al. (1988); Pucillo (2016, 2018); Lei and Feng (2004); Lim et al. (2003, 2008); El-Ghazaly et al. (1991). By this approach, the track structure is reduced to a discrete system of finite elements while the ballast constraining actions on the sleepers are schematically represented by non-linear springs whose characteristics have to be experimentally determined as reported in De Iorio et al. (2014a,b,c, 2017); Pucillo et al. (2018). However, numerical models are not able to explain by a concise mathematical language the effects of the geometrical and mechanical parameters on the track critical conditions. Consequently, they are ill-suited for helping the railway engineer that has to make design and strategic choices on the base both of its direct experience and data gathered from the track installation site. An analytical track model could be a valid alternative, since it offers a synthetic representation of the essential properties of the track and provides in a form useful by a technical point of view the actual knowledge state about the track behaviour. Yet, the attempts made by the researchers to build accurate analytical track models are very few.

In many of the models till now proposed it is assumed that track in the lateral plane acts like a Bernoulli-Euler beam having bending stiffness equal to twice the minimum bending stiffness ($E_rI_r$) of each rail (Kerr (1978a); Tvergaard and Needleman (1981); Martínez et al. (2015); Yang and Bradford (2016), for example). Into a second modelling approach, the inner bending moment is instead evaluated by adding two terms: the first term is generated by the curvature changes of the rails and is proportional to $2(E_rI_r)$, the second one is due to the constraint action the fasteners exert on the rails, see Kerr (1978b); Zakeri (2012). The main shortcoming of these kinds of models is that they do not take into account the effects of both the bending stiffness of the sleepers and the track gauge.

To overcome this limitation, Kerr and co-workers, observing that the track is a periodic beam-like structure built by repetitive assembling of two dimensional elements, in Kerr and Zarembki (1981); Kerr and Accorsi (1987); Grissom and Kerr (2006) have developed a continuous model adopting an homogenization technique based on finite differences approximation . Instead, according to the model of Zhu-Attard the track in the lateral plane behaves as a sandwich beam, Zhu and Attard (2015).

In this work, a new one-dimensional continuous model is developed by a homogenization method based on the eigen- and principal vectors of the unit cell transfer matrix. Closed forms for deformation modes of the unit cell by which the inner forces are transferred through the track are determined by the direct method reported in Penta et al. (2017); Gesualdo et al. (2018b). In order to identify the equivalent continuum, an energetic approach has been developed, without any *a priori* assumption on the kinematics of both the track and its substitute medium.

The proposed model can approximate the track behaviour in transferring the inner forces and, as it will be shown, is able to satisfy only a limited set of boundary conditions for end nodal and sectional rotations. For taking into account the local effects of the transversal loads and extending the applicability of the proposed model to more general boundary conditions, a corrective solution have to be superimposed. This latter is built by homogenizing the response of the unit cell to a system of inner self-equilibrated bending moments decaying through the track.

Lastly, the homogenization error due to the proposed approach has been evaluated by means of a sensitivity study carried out by the finite element method.

## 2. Track transmission modes

The adopted scheme of the periodic rail-tie structure is shown in Fig. 1 together with the unit cell. To simplify the analysis, we neglect the small angle that the rails longitudinal symmetry planes make with the vertical track symmetry plane. Moreover, we assume that rails and sleepers axis belong to the same horizontal plane. Thus, the considered track is a plane framework made up of straight parallel rails and equally spaced sleepers connected by means of springs of stiffness $k_\vartheta$ representing the fasteners.

In the analysis, the response of all the track elements is elastic while rails and webs of the unit cell are Bernoulli-Euler beams. The rails have area $A_r$ and minimum second order central moment of area $I_r$. The sleepers are assumed axially inextensible and have the second order moment equal to $I_s$. To respect the track periodicity, the second order area moments of the cell webs are equal to the half part of the second order area moment $I_s$, while the stiffness of the unit cell torsional springs is $k_\vartheta/2$.

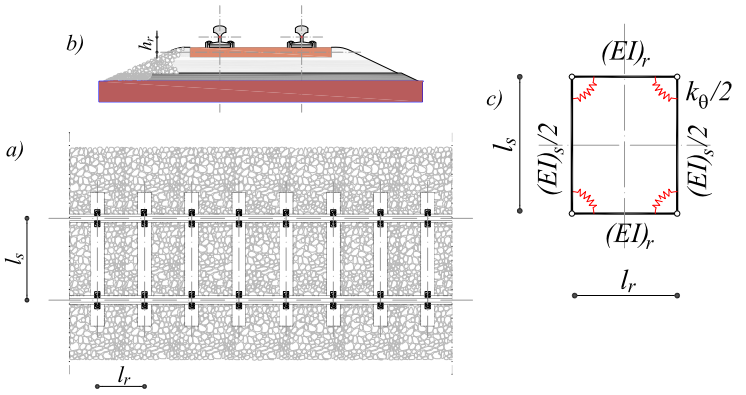


Figure 1. Schematic view of the elastically jointed rails-sleepers framework (a), track cross section (b) and unit cell (c).

To identify any quantity related to the track $i$-th nodal section, the sub-script $i$ will be adopted, see Fig. 2. To distinguish between the joints or nodes of the same section, the superscripts $t$ or $p$ are used, depending on whether the top or bottom rail is involved. Finally, in a coherent manner, top and bottom nodes of the section $i$ are labelled $i_t$ or $i_b$.

The static and kinematical quantities of the $i$-th cell are also schematically shown in Fig. 2. However, for our purposes, it is more convenient to adopt static and kinematic quantities alternative to the standard ones shown in this figure. More precisely, the deformed shape of the cell will be defined in terms of the mean axial displacement $\hat{u}_j = 1/2\left(u_j^t + u_j^b\right)$, the section rotation $\psi_j = \left(u_j^b - u_j^t\right)/l_t$, the transverse displacement $v_j$ and, finally, the symmetric and anti-symmetric parts of the section nodal rotations $\hat{\varphi}_j = 1/2\left(\varphi_j^t + \varphi_j^b\right)$ and $\tilde{\varphi}_j = 1/2\left(\varphi_j^t - \varphi_j^b\right)$.

The static quantities conjugates to the previous kinematic variables are: the axial force $n_j = (F_j^b + F_j^t)/2$, the bending moment $M_j = \left(F_j^b - F_j^t\right) l_t$ generated by the anti-symmetric axial forces, the shear force $V_j = F_{jy}^t + F_{jy}^b$, the resultant of the nodal moments $\hat{m}_j = m_j^t + m_j^b$ and, finally, the difference between the same moments $\tilde{m}_j = m_j^t - m_j^b$.

The state vector $\mathbf{s}$ of a track nodal cross section consists of its displacements vector $\mathbf{d}$ and the vector $\mathbf{f}$ of the forces that the section transfers. Hence, the state vectors of the end sections of the $i$ cell are $\mathbf{s}_{i-1} = \left[\mathbf{d}_{i-1}^T, \mathbf{f}_{i-1}^T\right]^T$ and $\mathbf{s}_i = \left[\mathbf{d}_i^T, \mathbf{f}_i^T\right]^T$, Fig. 2. They are related by the transfer matrix $\mathbf{G}$:

$$\mathbf{G}\,\mathbf{s}_{i-1} = \mathbf{s}_i\,.$$

As shown in Stephen and Wang (1996, 2000), the force transmission modes of the unit cell are given by the unit principal vectors of the $\mathbf{G}$ matrix. By the direct approach proposed in Penta et al. (2017), the problems due to the ill-conditioning of $\mathbf{G}$ are altogether avoided since principal vectors are determined in closed form by operating directly on the unit cell stiffness matrix.

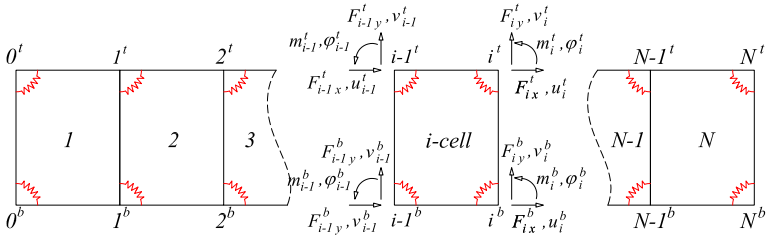


Figure 2. Unit cell nodes numbering and positive static and kinematical quantities.

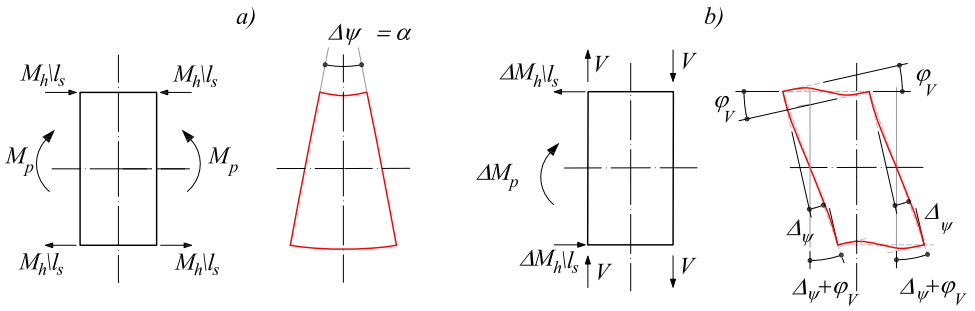


Figure 3. Forces subvector components and unit cell deformed shapes of bending moment (a) and shear forces (b) transmission modes.

The principal vector $\mathbf{s}_b$ pertaining to the pure bending mode has displacement and force sub-vectors respectively given by:

$$\mathbf{d}_b = 1/2\,[\,0,\ \alpha,\ 0,\ \alpha,\ 0\,]^T, \qquad \mathbf{f}_b = \alpha\,[\,0,\ \beta_r/2,\ 0,\ 2\eta_r,\ 0\,]^T \tag{1}$$

where $\alpha$ is the rigid unit cell rotation, $\beta_r = E_r A_r l_s^2/l_r$ and $\eta_r = E_r I_r/l_r$. Eq. (1) indicates that due to bending, the top and bottom nodes of the unit cell rotate exactly of the same angle as the cross section they belong to does. In other words, the cell transfers the bending moments without deformations of the webs (Fig. 3). This result was already observed in Gesualdo et al. (2017) by numerical experimentation on Vierendeel girders unit cells. In addition, two bending moments are transferred through the unit cell: the first one, to which we refer as primary bending moment, is generated by the couple of axial forces acting on the rails, the second one, to which instead we refer as secondary or micro-polar moment, is exclusively due to curvature change of the rails and is given by the resultant of the nodal moments.

The principal vector $\mathbf{s}_V$ defining the shear transmission mode is generated by $\mathbf{s}_b$ and has displacements and forces sub-vectors respectively given by

$$\mathbf{d}_V = \left[0, \Delta_\psi + \varphi_V, 0, \varphi_V, 0\right]^T, \qquad \mathbf{f}_V = \alpha \left[0, -\frac{\beta_r}{2}, \frac{\beta_r/2 + 2\eta_r}{l_r}, -2\eta_r, 0\right]^T$$

where

$$\Delta_\psi = \frac{\alpha}{48}\frac{\beta_r}{\eta_t}, \qquad \varphi_V = \frac{\alpha}{48}\left(\frac{\beta_r}{\eta_r} + 8\right)$$

with $\eta_s = (E_s I_s)\,/\,[l_s\,(6\alpha_s - 1)]$ and $\alpha_s = (E_s I_s)\,/\,(k_\vartheta l_s) + 1/3$.

The deformed shape of the unit cell due to the shear transmission mode is schematically depicted in Fig. 3(b) assuming that $\Delta v_i = v_{i+1} - v_i = 0$. Actually, this shape is obtainable by superposition of two independent modes. The first one, shown in Fig. (4a), involves rigid rotation of the sleepers and skew bending deformation of both rails, whose end sections rotate exactly of the same angle as the sleepers do. Consequently, it generates respectively the transversal shear forces

$$V = \pm\, 24\frac{\eta_c}{l_r}\left(\bar{\psi} - \frac{\Delta v}{l_r}\right),$$

with $\bar{\psi}$ rotation angle of the cell webs, and the secondary bending moments $\mp\, 12\,\eta_r\,(\bar{\psi} - \Delta v/l_r)$ applied on the left and right sides of the cell. The second deformed shape involved in shear transmission is instead associated with the relative rotation $\xi = (\psi - \varphi)$ of the cell nodal sections with respect to the mean nodal rotation $\varphi$. It does not produce any transversal shear (Fig. 4b) and is characterized by rigid translations of the rails and flexural deformation only of the sleepers. Their end sections in this mode does not rotate but carry out a relative transversal displacement equal to $(\psi - \varphi)\,l_s$. The related distorting forces acting on each cell face are a couple of axial forces $N_V = \pm 12\ (\eta_s/l_s)\,(\psi - \varphi)$ and two nodal moments $6\,\eta_s\,(\psi - \varphi)$ equilibrating the primary bending moment generated by the forces $N_V$. It is noteworthy that, as consequence of the previous forces system, an uniform horizontal shear $S_H = N_V$ is induced in each sleeper.

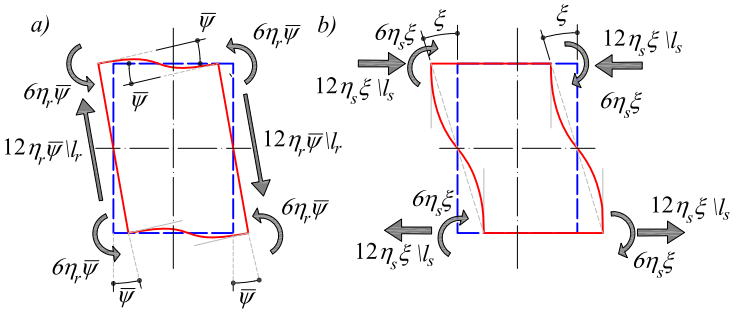


Figure 4. Unit cell deformations generating the transversal (a) and the longitudinal (b) shears.

Finally, the components $\mathbf{d}_a$ and $\mathbf{f}_a$ of the axial force transmission mode $\mathbf{s}_a$ are:

$$\mathbf{d}_a = [\,¿,\,0,\,¿,\,0,\,0\,]^T, \qquad \mathbf{f}_a = \tilde{u}\,[\,\beta_a,\,0,\,0,\,0,\,0\,]^T$$

where $\beta_a = (2\beta_r)/(l_r l_s^2) = 2E_r A_r/l_r$, $\tilde{u}$ denotes a rigid unit cell translation in the axial direction and the symbol ¿ is adopted for indeterminate quantities.

## 3. Track continuum model

In order to write the expression of the cell strain energy associated with the inner forces transmission modes, we adopt the following re-parametrization of the sectional and nodal rotations:

$$\psi = \bar{\psi} + \xi, \qquad \varphi = \bar{\psi},$$

where $\bar{\psi}$ is the common part of $\psi$ and $\varphi$ due to both bending and transversal shear while $\xi$ is the difference $\psi - \varphi$ caused by the longitudinal shear. Furthermore, we decompose the unit cell response to the shear and bending moment in the three following parts: pure bending, symmetric bending due to shear and antisymmetric bending and shear (Fig. 5). Then, denoting by $\Delta(.)$ the change of a generic quantity $(.)$ over the cell range, the cell strain energy due to the transmission modes is written as:

$$E_u = \frac{1}{2}\left(\frac{\beta_r}{2} + 2\eta_r\right)\Delta\bar{\psi}^2 + E_s + 12\eta_r\left(\bar{\psi} - \frac{\Delta v}{l_r}\right)^2 + 12\eta_t\,\xi^2 + \frac{1}{2}\beta_a\Delta u^2.$$

where $E_s$ is the strain energy pertaining to the symmetric bending due to shear.

A 1-D equivalent continuum for the track can be built by the following two-steps procedure. Firstly, the elastic strain energy $\bar{E}$ per (track) unit length is evaluated by dividing the unit cell energy $E_u$ by the cell length $l_r$. Then, considering that $l_r$ is usually very smaller than the length $L$ of the track to be analysed or equivalently that $\varepsilon = l_r/L \ll 1$, the ratios $\Delta\bar{\psi}/l_r$, $\Delta v/l_r$ and $\Delta u/l_r$ may be interpreted as the incremental ratios of the differentiable functions $\bar{\psi}(x)$, $v(x)$ and $u(x)$ that define together with $\xi(x)$ the deformed shape of the substitute medium. Consequently, they may be approximated

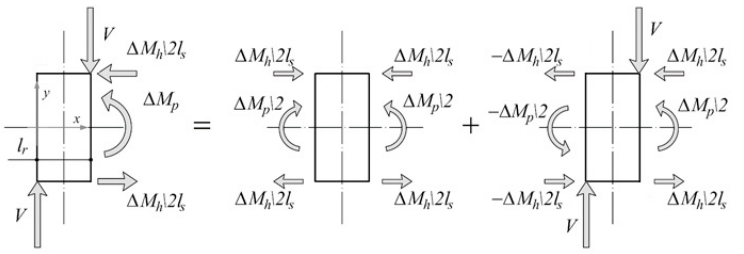

Figure 5. Decomposition of shear and bending moment change in symmetric and antisymmetric parts.

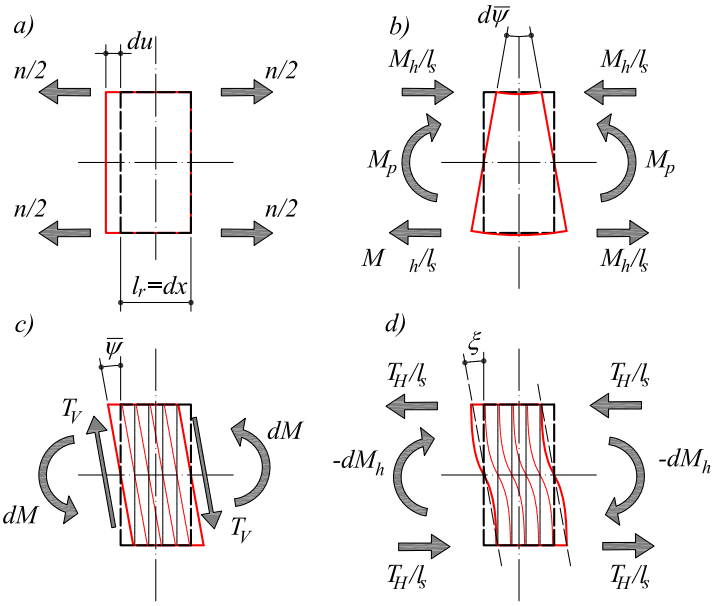


Figure 6. Deformed shapes of the elementary cell due to axial force (a), bending (b), transversal shear (c) and longitudinal shear (d).

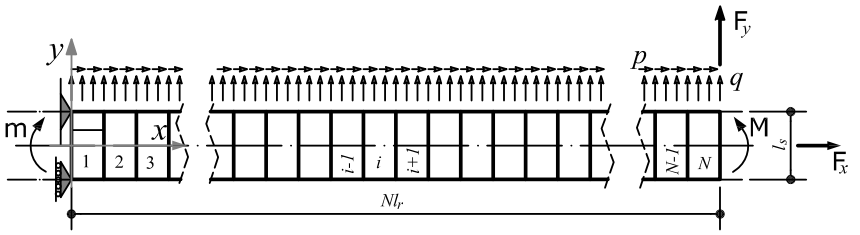


Figure 7. Track segment under axial and transversal loads.

by their limit as $\varepsilon \to 0$, namely by the first derivatives of these functions. In addition, the strain energy $E_s$ as $\epsilon \to 0$ is an higher order infinitesimal quantity and for this reason disappears. Thus, the following expression of the elastic strain energy density $E$ of the equivalent continuum is obtained:

$$E = \frac{1}{2}\left(\Gamma_h + \Gamma_p\right)\left(\frac{\mathrm{d}\bar{\psi}}{\mathrm{d}x}\right)^2 + \frac{1}{2}\kappa_V\left(\bar{\psi} - \frac{\mathrm{d}v}{\mathrm{d}x}\right)^2 + \frac{1}{2}\kappa_H\xi^2 + \frac{1}{2}\kappa_a\left(\frac{\mathrm{d}u}{\mathrm{d}x}\right)^2 \tag{2}$$

where $\Gamma_h = \beta_r l_r/2$ and $\Gamma_p = 2\eta_r l_r$ are respectively the primary and secondary (or micro-polar) bending stiffness's, $\kappa_a = \beta_a l_r$ is the axial stiffness and, finally, $\kappa_V = 24\eta_r/l_r$ and $\kappa_H = 24\eta_t/l_r$ are the transversal and longitudinal shear stiffness's.

When $\varepsilon \ll 1$ the real track may be approximated by a continuous fictitious one, composed of elementary cells of length $dx = l_r$ having properties analogous to those of the unit cell analysed in previous section (Fig. 6b). They transmit the primary and micro-polar bending moments $M_h$ and $M_p$ involving only a $d\bar{\psi}$ change, namely maintaining undeformed the transversal fibres or equivalently conserving the cross sections plane.

Regarding the shear property of the equivalent track, we may imagine that the transversal shear is generated by elastic sliding of cross sections that remain plane during deformation or equivalently by sliding of the undistorted transversal fibres, Fig. 6c. The longitudinal shear, that is equilibrated by the primary bending moment changes, is instead due to the skew symmetric bending of these fibres about the system axis.

The equilibrium equations of the substitute medium are straightforwardly obtained by invoking the principle of virtual works. As an example, we consider the case of the track segment constrained as the cantilever of Fig. 7 and subjected to the distributed axial and transversal loads $p$ and $q$, respectively. At the free end, a concentrated force of

components $\mathsf{F}_x$, $\mathsf{F}_y$ and the bending couple $\mathsf{M}$ are applied. Equating the virtual works of the inner and external forces due to kinematically admissible changes of $u$, $v$, $\xi$ and $\bar{\psi}$ and integrating by parts the term containing first derivatives of the changes, we obtain the following equilibrium conditions for the inner points of the equivalent track:

$$\Gamma_h \frac{\mathrm{d}^2\bar{\psi}}{\mathrm{d}x^2} = \kappa_H \xi, \qquad \Gamma_b \frac{\mathrm{d}^2\bar{\psi}}{\mathrm{d}x^2} = \kappa_V \left(\bar{\psi} - \frac{\mathrm{d}v}{\mathrm{d}x}\right), \qquad \kappa_V \left(\frac{\mathrm{d}\bar{\psi}}{\mathrm{d}x} - \frac{\mathrm{d}^2 v}{\mathrm{d}x^2}\right) = q, \qquad \kappa_a \frac{\mathrm{d}^2 u}{\mathrm{d}x^2} + p = 0, \tag{3}$$

while at the boundaries the following equalities must holds:

$$\begin{aligned} &\psi|_{x=0} = \bar{\psi}\big|_{x=0} + \xi|_{x=0} = 0, && v|_{x=0} = 0, && u|_{x=0}, \\ &\Gamma_p \frac{\mathrm{d}\bar{\psi}}{\mathrm{d}x}\bigg|_{x=0} = \mathsf{m}, && \Gamma_b \frac{\mathrm{d}\bar{\psi}}{\mathrm{d}x}\bigg|_{x=L} = \mathsf{M}, && \kappa_a \frac{\mathrm{d}u}{\mathrm{d}x}\bigg|_{x=L} = \mathsf{F}_x, \quad \kappa_V \left(\bar{\psi} - \frac{\mathrm{d}v}{\mathrm{d}x}\right)\bigg|_{x=L} = \mathsf{F}_y. \end{aligned} \tag{4}$$

with $\Gamma_b = \Gamma_h + \Gamma_p$. The first of equations (3) expresses the equilibrium between the couple $T_H = \kappa_H \xi$ and the unitary change of the primary bending moment, Fig. 6d . The remaining equations are instead the in-plane rotational and translational equilibrium conditions of the unit length continuum segment.

It is worth noting that Eq. (3) make sense and give accurate predictions of the real track behaviour, only when boundary conditions and applied loads are such that the cells are allowed to deform according to the force transmission modes. If this condition is not satisfied a corrective solution has to be superimposed to the one obtained from (3). More details on this point are given in Sec. 5.

The Eq.(3) are very similar to the equilibrium equations of a Timoshenko couple-stress beam proposed by Ma et al. (2008), which is frequently adopted as substitute continuum for Vierendeel girders Gesualdo et al. (2017); Romanoff and Reddy (2014); Romanoff et al. (2016). In addition, Eq. (3) well highlight that it is essential to consider separately the contributions to bending moment due to the rail axial forces and bending, even though this second contribution in some cases is very small. If this is not the case, it would be not possible to model consistently the real track shear behaviour.

## 4. Self-equilibrated bending eigenvector

To improve the continuous model accuracy, also the eigenvectors $\mathbf{s}_\mu$ di $\mathbf{G}$ defining self-equilibrated systems of bending moments of amplitude $\mu$ decaying along the track have to be considered. They may be readily determined by the method reported in Penta et al. (2017); Gesualdo et al. (2018b). The corresponding eigenvectors are the root's of the following quadratic equation:

$$\lambda^2 - \left(2 + 12\,\frac{\eta_t}{\eta_r} + 48\,\frac{\eta_t}{\beta_r}\right)\lambda + 1 = 0.$$

Since the known term is equal to the unit, the eigenvectors occur as a reciprocal pair, according to whether the moments system decay from left to right, or vice versa. The displacements and forces components of the eigenvector associated to the eigenvalue greater than unity are given by

$$\mathbf{d}_\mu = \frac{\mu}{\Delta_\mu}\left[0, 2\eta_r, 0, -\frac{1}{2}\beta_r, 0\right]^T, \qquad \mathbf{f}_\mu = [0,\, \mu, 0,\, -\mu,\, 0]^T$$

with $\Delta_\mu = \beta_r \eta_r\,(\lambda - 1) - 6\eta_s\,(\beta_r + 4\eta_r)$. The displacement components corresponding to the eigenvalue lesser than unity can be derived from the previous ones by simple symmetry considerations. By means of previous results, the deformed shape of a track made of $N$ cells constrained as the cantilever of fig. 8 in which self-equilibrated bending moments are vanishing can be built by kinematical composition of its unit cells strains. In the case of unit self-equilibrated

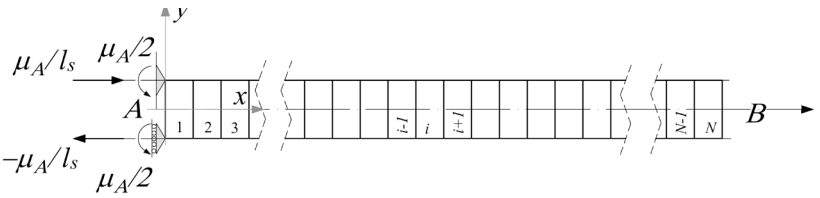


Figure 8. Track segment under self-equilibrating bending moments decaying from left to right.

bending moments on the track constrained section and unloaded free end, for the rotations $\psi_i$, the displacement $v_i$ and the nodal rotation $\varphi_i$ of the $i$ section one obtains:

$$\begin{aligned}
\psi_i &= \frac{\Delta\psi_{(+)}\left(\tilde{\lambda}^i-1\right)\left(\tilde{\lambda}^{2\Lambda-i}-1\right)}{\left(\tilde{\lambda}-1\right)\left(\tilde{\lambda}^{2\Lambda}-1\right)},\\
\varphi_i &= \frac{1}{2}\frac{2\tilde{\lambda}^{2\Lambda}-\left(\tilde{\lambda}+1\right)\tilde{\lambda}^{\Lambda}-\tilde{\lambda}+1}{\left(\tilde{\lambda}-1\right)\left(\tilde{\lambda}^{2\Lambda}-1\right)}\Delta\psi_{(+)}-\frac{1}{2}\frac{2\tilde{\lambda}^{i}-\left(1+\tilde{\lambda}\right)\left(\tilde{\lambda}^{\Lambda}+1\right)+2\tilde{\lambda}^{2\Lambda-i}}{\left(\tilde{\lambda}-1\right)\left(\tilde{\lambda}^{2\Lambda}-1\right)}\Delta\varphi_{(+)}+\frac{\tilde{\lambda}^{\Lambda}+1}{\tilde{\lambda}^{2\Lambda}-1}\gamma_{\psi(+)},\\
v_i &= \frac{\Delta\psi_{(+)}l_r}{\left(\tilde{\lambda}-1\right)^2\left(\tilde{\lambda}^{2\Lambda}-1\right)}\left[i\left(\tilde{\lambda}^{2\Lambda}+1\right)\left(\tilde{\lambda}-1\right)+-1/2\left(\tilde{\lambda}^{i}-1\right)\left(1+\tilde{\lambda}\right)\left(\tilde{\lambda}^{2\Lambda-i}+1\right)\right]+\gamma_{\psi(+)}l_r\frac{\left(\tilde{\lambda}^{i}-1\right)\left(\tilde{\lambda}^{2\Lambda-i}+1\right)}{\left(\tilde{\lambda}-1\right)\left(\tilde{\lambda}^{2\Lambda}-1\right)}.
\end{aligned} \tag{5}$$

being $\Lambda = N = L/l_r$ and $\tilde{\lambda} = \lambda^{-1}$. For reason of brevity, the procedure adopted to derive previous results is not reported. A rigorous proof of eq.(5) will be given in a forthcoming paper.

From previous results, a continuous approximation of the track response may be achieved by considering the limit case of unit-cell having infinitesimal length (with respect to the track length). This continuous track solution can be achieved observing that

$$\tilde{\lambda}^i = \left[1-\left(\tilde{\lambda}-1\right)\right]^i = \left[1+\frac{\left(\tilde{\lambda}-1\right)}{l_r}\frac{x_i}{i}\right]^i, \tag{6}$$

with $x_i = i\,l_r$ abscissa of the nodal section $i$ in the reference frame of Fig. 8. When the cell sizes are very smaller than the track length $L$ or equivalently the track is composed of a great number of cells per unit length, it will result in

$$x_i >> l_r \quad \text{and} \quad i >> 1. \tag{7}$$

Under these conditions, to the last quantity in Eq. (6) we may substitute the corresponding limit as $i$ approaches $+\infty$:

$$\left[1+\frac{\left(\tilde{\lambda}-1\right)}{l_r}\frac{x_i}{i}\right]^i \simeq e^{(\tilde{\lambda}-1)\zeta_i} \tag{8}$$

with $\zeta_i = x_i/l_r$. When this limit value is inserted in Eq. (5) and the variable $\zeta_i$ is substituted by the non-dimensional real variable $\zeta$ ranging in $[0, \Lambda]$, three continuous functions $\psi$, $\varphi$ and $v$ are obtained. These latter define the deformed shape of a continuum equivalent medium, that may be thought as an asymptotic approximations of the track behaviour, exact only in the limit when $i \to +\infty$.

## 5. Track analysis

By means of the equivalent continuum of Sec. 3 and the approximating solution of Sec. 4, the track behaviour for quite simple constraint and loading cases can be readily analysed.

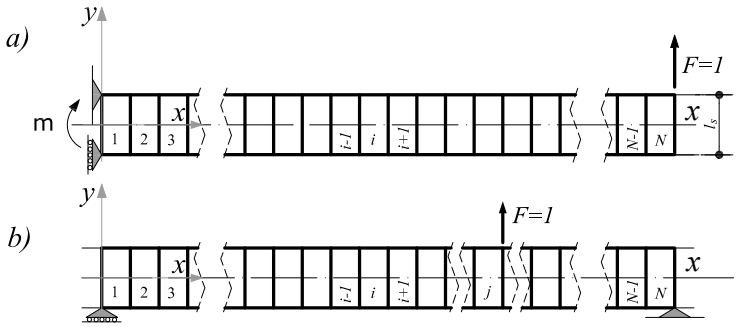


Figure 9. Track segment under different loading and constraint conditions: (a) clamped end and unit transversal force at the free end, (b) simply supported with a unit transversal load on the j-th sleeper.

*Case 1 - Track with a clamped end.* As first example, we examine the behaviour of a track made of $N$ cells constrained as shown in Fig. 9-a and loaded by a unit transversal load at the free end. Initially, we assume that only the cross-section rotation $\psi$ at $x = 0$ is blocked by the constraint and that the nodal moment $\mathsf{m} = (\Gamma_p/\Gamma_b)L$ is applied on this section. The solution of this boundary value problem is obtained by integrating the equilibrium equations (3). Since at $x = 0$ only the sectional rotation is constrained, a nodal rotation $\varphi_0 = \Gamma_h/(\Gamma_b\kappa_H) \neq 0$ occurs.

If, instead, the boundary conditions at $x = 0$ are formulated also in terms of the symmetric nodal rotations $\varphi$, the previous solution has to be corrected by adding to it a self-equilibrated one derived from Eq. (5). From this latter equation, the following expression of the direct nodal rotational compliance $\delta_\varphi$ at the constrained section is also derived:

$$\delta_\varphi = \frac{\Gamma_b}{\Delta_\eta}\frac{\exp\left[(\lambda-1)\,2L/l_r\right]+1}{\exp\left[(\lambda-1)\,2L/l_r\right]-1}. \tag{9}$$

Thus, denoting by $\bar{\varphi}$ the prescribed value of $\varphi$ at $x = 0$, the constraint has to transfer to the track also the nodal moment $m_0$ given by:

$$m_0 = \frac{\Delta_\eta}{\Gamma_b}\frac{\exp\left[(\lambda-1)\,2L/l_r\right]-1}{\exp\left[(\lambda-1)\,2L/l_r\right]+1}\,(\bar{\varphi}-\varphi_0)$$

in order to the boundary conditions for $\varphi$ be satisfied.

*Case 2 - Simply supported track with unit transversal load.* By means of the results achieved for the Case 1, it is possible to build an approximation for the response of a simply supported track under a unit transversal load. For this purpose, we examine the 2D system of Fig. 9b composed of $N$ cells and subjected to a unit transversal load applied on the upper end of the $j$-th sleeper.

It is convenient to analyse preliminary the effect of this loading condition on the response of a discrete track. We recall that when a cell deform by bending or transversal shear, its transversal webs remain undeformed. Hence, generalized strains associated to these two kinds of inner forces are always geometrically compatible. Geometrical incompatibility, instead, takes place if the longitudinal shear varies from a cell to the next one. This happens when a transversal load is applied on a sleeper. In Fig. 10, the deformed shapes assumed by the cells $i$ and $i + 1$ as a consequence of the strains due to different longitudinal shears are represented under the assumption that they are mutually constrained by hinges. In the common nodal section, the transversal beams of the two cells does not have the same deformed shape, so that a jump $\Delta\varphi$ in the nodal rotation occurs. In order to restore the continuity without violating the equilibrium, the two cells have to interact also by a self-equilibrated bending moments system. This will generate relative rotations between the coincident nodes of the cells such that the previous jump $\Delta\varphi$ disappears.

In close analogy with the discrete problem, we may build the continuous approximation of the track response by superimposing two solutions. The first one, defined by Eq. (3) and b.c. of Fig. 9b, represents the effect of the transmission through the cells of the inner forces in equilibrium with the external load. The second one is generated by the self-equilibrated bending moments needed to eliminate the jump in the nodal rotations caused by the applied

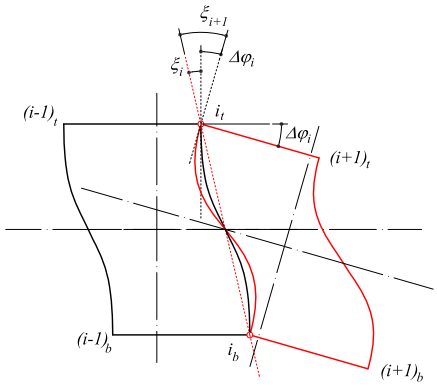


Figure 10. Deformed shapes of two adjacent cells under different longitudinal shears

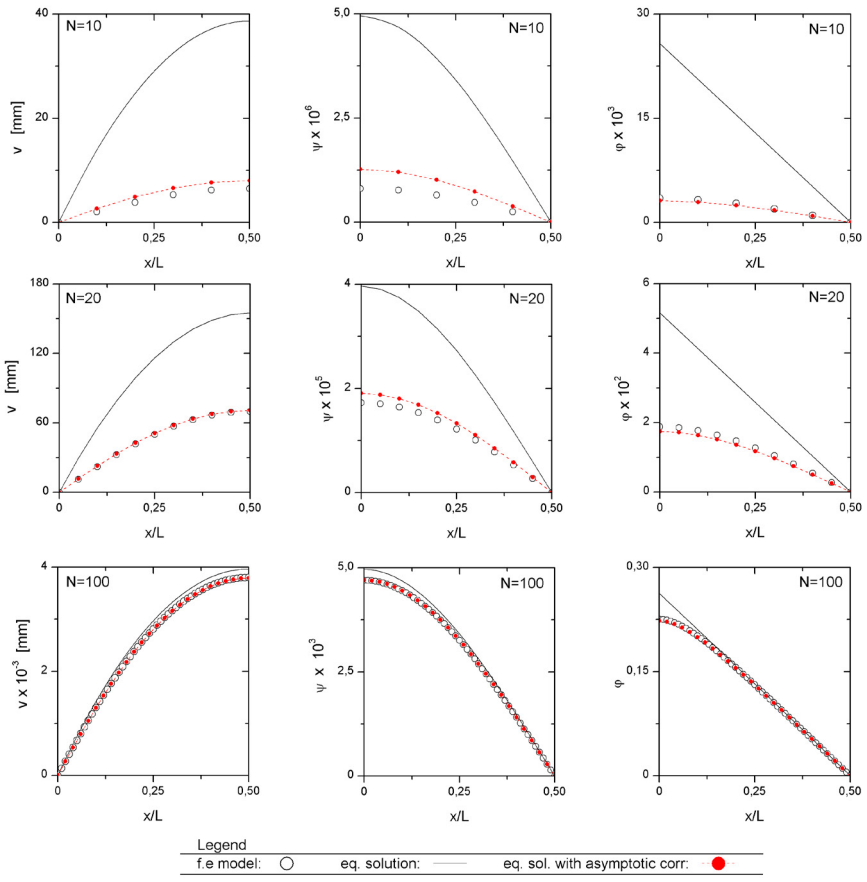


Figure 11. Theoretical and numerical predictions of the displacements (*left column* ), sectional rotations (*central column*) and nodal rotations ( *right column* ) of track segments with N = 10, 20 and 100 cells.

transversal load. In order to determine the amplitude $m_1$ of this couple of bending moments, we observe that in the equilibrated solution the unit transversal load causes the jump $\Delta T_H = \Gamma_h/\Gamma_p = \alpha_H$ in the couple $T_H = dM_h/dx$. Hence, according to the first of Eq. (3) for the nodal rotations of the section $j$ where the load is applied the discontinuity

$$\Delta\varphi = -\Delta\xi = -\Delta T_H/\kappa_H \tag{10}$$

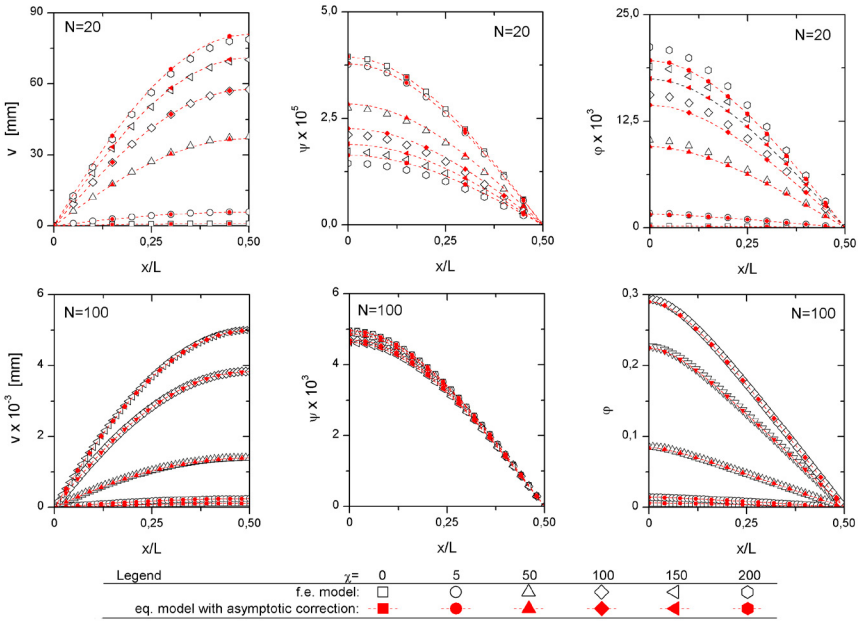


Figure 12. Effects of changes in fasteners stiffness on the response of track segments with $N = 20$ (*upper row*) and $N = 100$ (*lower row*) cells .

takes place. To eliminate it, we introduce in the loaded section two hinges to constrain the nodes of the contiguous elementary cells. Then on the right and left side parts of the section $j$ we apply self-equilibrated bending moments of intensity $\mathsf{m}_1$ such that the jump $\Delta\varphi_1 = -\Delta\varphi$ for the nodal rotations occurs. By the compliance given in Eq. (9) and taking into account the signs of the nodal rotations caused by a positive self-equilibrated moment at the left and right hand side of the loaded section, for the jump $\Delta\varphi_1$ we obtain:

$$\Delta\varphi_1 = \mathsf{m}_1 \frac{2\Gamma_b}{\Delta_\eta} g\left(x_f\right), \tag{11}$$

where

$$g\left(x_f\right) = \frac{\left\{\exp\left[2\left(\lambda-1\right)L/l_r\right]-1\right\}}{\left\{\exp\left[2\left(\lambda-1\right)\left(L-x_f\right)/l_r\right]-1\right\}\left\{\exp\left[2\left(\lambda-1\right)x_f/l_r\right]-1\right\}}.$$

Hence, the self-equilibrated bending moment active in the loaded section is

$$\mathsf{m}_1 = \frac{1}{48}\frac{\alpha_H\Delta_\eta}{\kappa_H\Gamma_b} g\left(x_f\right)^{-1}. \tag{12}$$

Both equilibrated and self-equilibrated solutions to be superimposed are obtained by combining the results achieved for the cantilever of Case 1 by a procedure analogous to the one usually adopted for simply supported Euler-Bernoulli beams.

## 6. Homogenization Error and Validation Study

To examine in detail the homogenization errors of the interpolating and asymptotic approximations, a sensitivity study has been carried out. For this purpose, a track with the following geometrical and mechanical properties, has been considered:

$$\begin{aligned} &l_s = 1500 \text{ mm}, \quad && l_r = 600 \text{ mm}, && k_\theta = 3.5{\times}10^7 \text{ Nmm} \\ &A_r = 7670 \text{ mm}^2, && I_r = 5.123{\times}10^6 \text{ mm}^4, && I_s = 2.50{\times}10^8 \text{ mm}^4 \end{aligned} \tag{13}$$

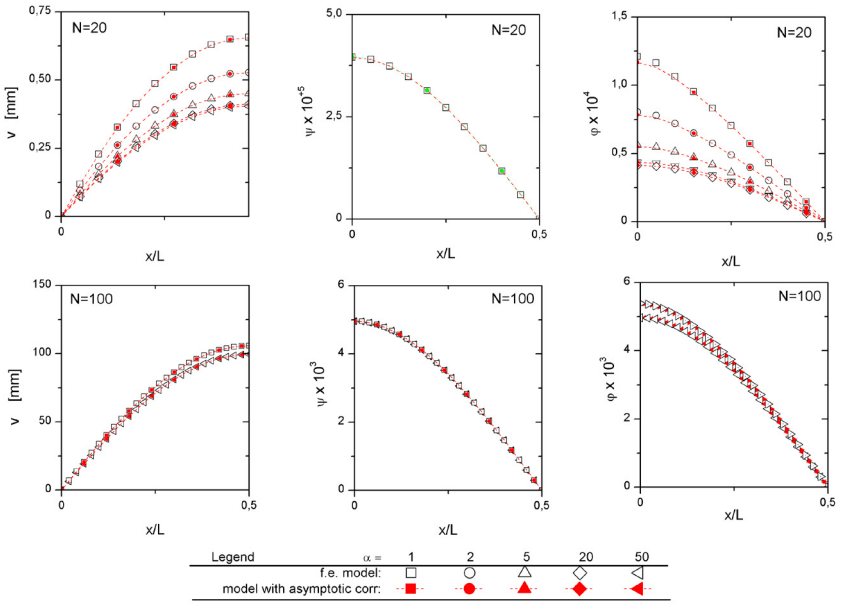


Figure 13. Effects of changes in sleeper second order moment on the response of track segments with $N = 20$ (*upper row*) and $N = 100$ (*lower row*) cells.

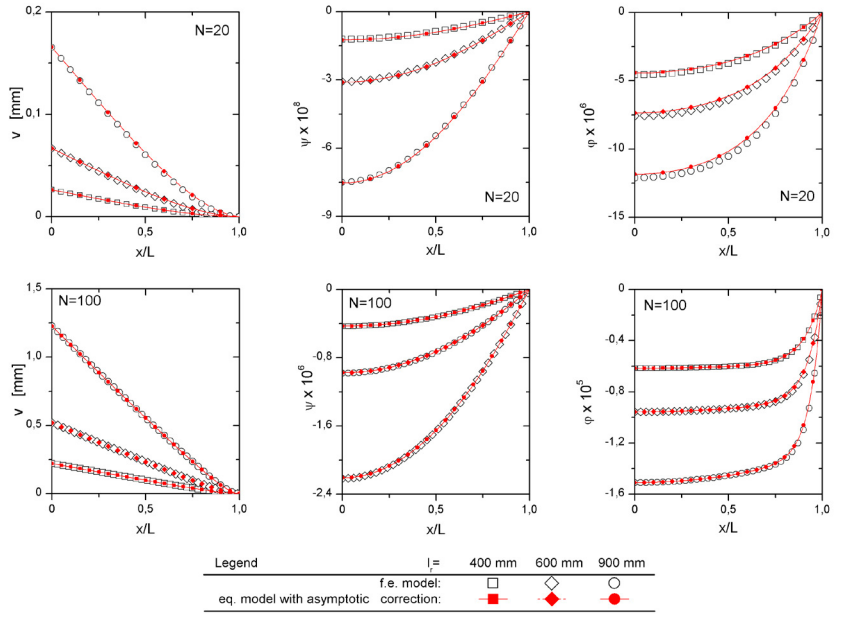


Figure 14. Effects of changes in sleepers spacing on the response of track segments with $N = 20$ (*upper row*) and $N = 100$ (*lower row*) cells.

and the accuracy of the proposed models has been analysed changing once or twice per time the values of these parameters. Indeed, a track having properties given in Eq. (13) may be thought as representative of a high speed tangent track of the Italian Railway Network.

By considering a series of track composed of a number $N$ of unit cells increasing from 10 until 100, the range of $\varepsilon$ values where the continuum model is applicable is investigated . The static scheme adopted is a simply supported beam under a unit uniform load. The predictions of the theoretical model were obtained by integrating with respect to the abscissa of the loaded track section the results achieved for Case 2. All the needed computations were made in a

Computer Algebra System. Corresponding results are reported in the diagrams of Fig. 11 together with the ones of the F.E. simulations.

As can be seen from Fig. 11, the homogenization error, as expected, is strongly dependent on the cell number composing the track. It quickly decreases as the cell number increases, becoming negligible for the case of the displacement function $v$ as $N$ reaches the threshold value of 20 cells; for the rotations $\psi$ and $\varphi$ instead is necessary that $N$ exceeds the value of 50 cells, in order that the approximation become accurate.

In Fig. 12, the effects of the variations in torsional stiffness $k_\vartheta$ of the fasteners are reported. In fact, the frame parameter of the diagrams in this picture is the relative change $\chi = (3E_sI_s) / (l_sk_\vartheta)$ of the direct bending compliance of a simply supported sleeper equipped with its fasteners. In all the examined cases, the homogenization error is surprisingly small. Hence, we may affirm that the continuous model predicts with high accuracy the effects of the stiffness $k_\vartheta$ on the track equilibrium shapes.

The effects of the changes in the sleeper second order moment are negligible when the constraints between sleepers and rails have stiffness of the same order of magnitude as the torsional stiffness value given in Eq. (13). Under these conditions, varying $I_s$ does not affect significantly the direct bending compliance of the elastic system composed by sleepers and fasteners in series and consequently, the shear compliance of the unit cells. The effects of $I_s$ become instead substantial when the torsional stiffness $k_\vartheta$ has a very high value. In Fig. 13, the theoretical and numerical deformed track shapes, evaluated under the assumption of fasteners ideally rigid, are reported. The considered values of $I_s$ are $\alpha I_{s0}$ with $I_{s0}$ reference value given in Eq. (13) and $\alpha$ non-dimensional factor ranging in $[1, 50]$. It is evident that for all the examined values of $I_s$ and $N$, the homogenization errors are very small.

In Fig. 14 the effects of the sleeper spacing changes are shown. The considered static scheme is the cantilever-track having both nodal and section rotations blocked at $x = L$. Also in this case to have noticeably changes in the track response the assumption $k_\vartheta = +\infty$ is needed. For all the examined values of $N$ and $l_s$ the approximating solution well agree with the predictions from the F.E. models.

## Conclusions

A model for the mechanical behaviour of a tangent railway track in the lateral plane has been developed starting from the transmission modes of the unit cell. Their analysis reveals that bending moments are transferred through a unit cell without deforming the sleepers and fasteners. As a consequence, track bending moments are composed of two parts having fixed ratio: the first one is generated by the couple of axial forces acting in the rails, the other is due to bending moments of the rails. Solutions obtained from the proposed model are equilibrated but not kinematically admissible. To overcome the geometrical incompatibilities and improve the theoretical predictions accuracy, a corrective solution was derived from the eigenvectors of the unit cell transfer matrix pertaining to self-equilibrated systems of bending moments.

The accuracy of the approximations obtained by superposing the corrective solution has been analysed by a validation study carried out with some track F.E. models. In all the examined cases, the theoretical outcomes are very close to the numerical results when segments with more than 50 cells are considered. The homogenization procedure followed for the track model has great potential for analysing the dynamic isolation of fragile goods in tall buildings (i.e. art objects, see Gesualdo et al. (2018a)). It is also a serious candidate to analyse the buckling and post-buckling response of a railway track under thermal load. Further research has to be carried out to extend the presented results to both kinds of problems. Similarly, deeper studies are needed to apply the proposed technique also in the track elastic-plastic range, whereas the response of the unit cell has to be evaluated by approximated methods as those presented in Fraldi et al. (2014) and Cennamo et al. (2017).

## Acknowledgements

The Authors gratefully thank Eng. Mario Testa and Eng. Stefano Rossi, Technical Direction of Italian Railway Network (RFI S.p.A.), for their technical support and prof. Antonio De Iorio, University of Naples Federico II, for his valuable advices and warm encouragements.

## References


Cennamo, C., Gesualdo, A., Monaco, M., 2017. Shear plastic constitutive behavior for near-fault ground motion. Journal of Engineering Mechanics 143, 04017086.

De Iorio, A., Grasso, M., Penta, F., Pucillo, G.P., Pinto, P., Rossi, S., Testa, M., Farneti, G., 2014a. Transverse strength of railway tracks: part 1. Planning and experimental setup. Frattura ed Integrità Strutturale 30, 478–485. doi:10.3221/IGF-ESIS.30.58.

De Iorio, A., Grasso, M., Penta, F., Pucillo, G.P., Rosiello, V., 2014b. Transverse strength of railway tracks: part 2. Test system for ballast resistance in line measurement. Frattura ed Integrità Strutturale 30, 578–592. doi:10.3221/IGF-ESIS.30.69.

De Iorio, A., Grasso, M., Penta, F., Pucillo, G.P., Rosiello, V., Lisi, S., Rossi, S., Testa, M., 2014c. Transverse strength of railway tracks: part 3. Multiple scenarios test field. Frattura ed Integrità Strutturale 30, 593–601. doi:10.3221/IGF-ESIS.30.70.

De Iorio, A., Grasso, M., Penta, F., Pucillo, G.P., Rossi, S., Testa, M., 2017. On the ballast–sleeper interaction in the longitudinal and lateral directions. Proceedings of the Institution of Mechanical Engineers, Part F: Journal of Rail and Rapid Transit doi:0954409716682629.

El-Ghazaly, H., Sherbourne, A., Arbabi, F., 1991. Strength and stability of railway tracks – ii. Deterministic, finite element stability analysis. Computers & Structures 39, 23–45.

Esveld, C., Hengstum, L., 1988. Track stability in tight curves. Rail International 12, 15–20.

Fraldi, M., Gesualdo, A., Guarracino, F., 2014. Influence of actual plastic hinge placement on the behavior of ductile frames. Journal of Zhejiang University SCIENCE A 15, 482–495.

Gesualdo, A., Iannuzzo, A., Monaco, M., Penta, F., 2018a. Rocking of a rigid block freestanding on a flat pedestal. Journal of Zhejiang University-SCIENCE A 19, 331–345.

Gesualdo, A., Iannuzzo, A., Penta, F., Pucillo, G.P., 2017. Homogenization of a Vierendeel girder with elastic joints into an equivalent polar beam. Journal of Mechanics of Materials and Structures 12, 485–504.

Gesualdo, A., Iannuzzo, A., Pucillo, G.P., Penta, F., 2018b. A direct technique for the homogenization of periodic beam-like structures by transfer matrix eigen-analysis. Latin American Journal of Solids and Structures 15.

Grissom, G.T., Kerr, A.D., 2006. Analysis of lateral track buckling using new frame-type equations. International Journal of Mechanical Sciences 48, 21–32.

Jackson, J., Bauld, N., Ramesh, M., Menon, S., 1988. A superelement for lateral track deformation, in: Applied Mechanics Rail Transportation Symposium, ASME. pp. 7–17. Presented at the Winter Annual Meeting of the American Society of Mechanical Engineers, Miami Beach, Florida, November 17-22, 1985.

Kerr, A., Zarembki, A., 1981. The Response Equations for a Cross-Tie Track. Acta Mechanica 40, 253–76.

Kerr, A.D., 1978a. Analysis of thermal track buckling in the lateral plane. Acta Mechanica 30, 17–50.

Kerr, A.D., 1978b. Lateral buckling of railroad tracks due to constrained thermal expansions—a critical survey, in: Railroad track mechanics and technology, Elsevier. pp. 141–169.

Kerr, A.D., Accorsi, M.L., 1987. Numerical validation of the new track equations for static problems. International Journal of Mechanical Sciences 29, 15–27.

Lei, X., Feng, Q., 2004. Analysis of stability of continuously welded rail track with finite elements. Proc IMechE Part F: Journal of Rail and Rapid Transit 218, 225–233.

Lim, N., Han, S., Han, T., Kang, Y., 2008. Parametric study on stability of continuous welded rail track - ballast resistance and track irregularity. Steel Structures 8, 171–181.

Lim, N., Park, N., Kang, Y., 2003. Stability of continuous welded rail track. Computers & Structures 81, 2219–2236.

Ma, H., Gao, X.L., Reddy, J., 2008. A microstructure-dependent Timoshenko beam model based on a modified couple stress theory. Journal of the Mechanics and Physics of Solids 56, 3379 – 3391. URL: http://www.sciencedirect.com/science/article/pii/S002250960800152X, doi:https://doi.org/10.1016/j.jmps.2008.09.007.

Martínez, I.N., Sanchis, I.V., Fernández, P.M., Franco, R.I., 2015. Analytical model for predicting the buckling load of continuous welded rail tracks. Proceedings of the Institution of Mechanical Engineers, Part F: Journal of Rail and Rapid Transit 229, 542–552.

Penta, F., Monaco, M., Pucillo, G.P., Gesualdo, A., 2017. Periodic beam-like structures homogenization by transfer matrix eigen-analysis: A direct approach. Mechanics Research Communications 85, 81–88. doi:https://doi.org/10.1016/j.mechrescom.2017.08.007.

Pucillo, G., 2016. Thermal buckling and post-buckling behaviour of continuous welded rail track. Vehicle System Dynamics 54, 1785–1807.

Pucillo, G.P., 2018. On the effects of multiple railway track alignment defects on the cwr thermal buckling, in: 2018 Joint Rail Conference, American Society of Mechanical Engineers. pp. V001T01A018–V001T01A018.

Pucillo, G.P., De Iorio, A., Rossi, S., Testa, M., 2018. On the effects of the usp on the lateral resistance of ballasted railway tracks, in: 2018 Joint Rail Conference, American Society of Mechanical Engineers. pp. V001T01A017–V001T01A017.

Romanoff, J., Reddy, J., 2014. Experimental validation of the modified couple stress Timoshenko beam theory for web-core sandwich panels. Composite Structures 111, 130 – 137. URL: http://www.sciencedirect.com/science/article/pii/S026382231300620X, doi:https://doi.org/10.1016/j.compstruct.2013.11.029.

Romanoff, J., Reddy, J., Jelovica, J., 2016. Using non-local Timoshenko beam theories for prediction of micro- and macro-structural responses. Composite Structures 156, 410 – 420. URL: http://www.sciencedirect.com/science/article/pii/S0263822315005528, doi:https://doi.org/10.1016/j.compstruct.2015.07.010. 70th Anniversary of Professor J. N. Reddy.

Stephen, N., Wang, P., 1996. On Saint-Venant's principle in pin-jointed frameworks. International Journal of Solids and Structures 33, 79 – 97. URL: http://www.sciencedirect.com/science/article/pii/0020768395000197, doi:https://doi.org/10.1016/0020-7683(95)00019-7.

Stephen, N., Wang, P., 2000. On transfer matrix eigenanalysis of pin-jointed frameworks. Computers & Structures 78, 603

– 615. URL: http://www.sciencedirect.com/science/article/pii/S0045794900000365, doi:https://doi.org/10.1016/S0045-7949(00)00036-5.

Tvergaard, V., Needleman, A., 1981. On localized thermal track buckling. International Journal of Mechanical Sciences 23, 577–587.

Yang, G., Bradford, M.A., 2016. Thermal-induced buckling and postbuckling analysis of continuous railway tracks. International Journal of Solids and Structures 97, 637–649.

Zakeri, J.A., 2012. Lateral resistance of railway track, in: Reliability and safety in railway. InTech.

Zhu, J., Attard, M., 2015. In-plane nonlinear localised lateral buckling under thermal loading of rail tracks modelled as a sandwich column. International Journal of Mechanical Sciences 104, 147–161.